Arch. Metall. Mater. **71** (2026), 1, 399-410

DOI: https://doi.org/10.24425/amm.2026.157802

HONGYUAN SHENG[1,2], ZHIJUN HE[1,2], LIHUA GAO[1,2], XINYU YI[1,2], JIHUI LIU[1,2*]

TAILORING PELLET PERFORMANCE VIA BIOMASS ADDITIVES: STRENGTH ENHANCEMENT AND MICROSTRUCTURAL MODULATION

Against the backdrop of dwindling energy supplies and escalating environmental pressures in ironmaking, low-carbon ironmaking technologies have garnered significant research attention. This study centers on developing blast furnace biomass composite pellets from carbon-neutral biomass and high-silica magnetite concentrate. The physicochemical properties and pyrolysis behaviors of these biomass materials are systematically analyzed. From a microscopic structural perspective, the feasibility of forming spherical biomass composite pellets is critically discussed, followed by an in-depth examination of their strength and phase structure evolution. When the biomass addition ratio reaches 7%, the compressive strength of rice husk-waste wood chip composite pellets exceed 2200.00 $N \cdot P^{-1}$, while waste wood chip-based composite pellets exhibit a higher strength of 2660.03 $N \cdot P^{-1}$. High-temperature roasting of high-silica ore generates bridging solid solutions and minor complex silicates, which are dispersed within pores and between particles. This phenomenon enhances the structural integrity of composite pellets and reinforces their compressive strength. This work establishes a theoretical foundation for producing high-quality biomass composite pellets in blast furnace operations.

Keywords: Biomass; High silicon iron ore; Composite pellet; Microstructure changes

1. Introduction

Energy consumption is one of the key concerns for low-carbon production in iron and steel enterprises, where ironmaking energy consumption accounts for about 70% of the entire metallurgical process. Since the energy consumption of iron and steel mainly depends on fossil energy supply, a large amount of CO_2 is emitted during the smelting process, and the CO_2 emissions will exceed 1.8 billion tons in 2022 alone. Biomass is an important renewable carbon-containing energy source with wide distribution, large reserves, low content of harmful elements, low pyrolysis temperature, etc., which makes it a promising "carbon-neutral resource" [1-4]. There are more national and international reports on the use of biomass fuels as a substitute for coking coal in the iron and steel production process [5-8]. It is found that with the increase of the proportion of three biomass fuels, charcoal, burnt straw and moulded sawdust, which replace traditional coke powder in the sintering process, the sintering layer reaches a higher temperature in a short time, thus promoting the increase of vertical sintering speed and reducing the emission of CO, CO_2, SO_x and NO_x [9-15].

Cholico-González et al. [16] investigated the reduction behavior and degree of metallization of magnetite concentrate by agave bagasse under an inert atmosphere. XRD analysis showed that the degree of metallization increased with rising temperature and biomass content. Complete metallization was achieved within 30 min at 1100°C when the mass ratios of magnetite concentrate to agave bagasse were 65:35 and 50:50. Guo et al. [17] investigated the reduction mechanism and kinetics of CO-reduced biomass oxidation pellets. By adding biomass to increase the pellet porosity, the ingress and diffusion of CO were enhanced, accelerating the reduction extent of the pellets and shortening the total reduction time by 3%. Due to the presence of biomass, the pellets were further reduced by the biomass, so the activation energy required for reduction is changed from 87.30 $kJ \cdot mol^{-1}$ to 80.65 $kJ \cdot mol^{-1}$. Wei et al. [18] identified that the reduction of iron oxide by biomass char can be divided into two stages. The initial stage is dominated by volatile carbon, which is primarily controlled by gaseous diffusion. The subsequent stage is characterized by non-volatile carbon, which is predominantly influenced by carbon gasification. Ooi et al. [19] investigated the feasibility of utilising varying quantities of

[1] UNIVERSITY OF SCIENCE AND TECHNOLOGY LIAONING, SCHOOL OF MATERIALS AND METALLURGY, 114051, ANSHAN, LIAONING, CHINA
[2] KEY LABORATORY OF GREEN LOW-CARBON AND INTELLIGENT METALLURGY, LIAONING PROVINCE. 114051, ANSHAN, LIAONING, CHINA
* Corresponding author: jihuiliu240318@163.com

sunflower seed hulls as supplementary fuels in iron ore sintering experiments. Similarly, Takazo et al. [20] explored the potential of agricultural biomass in the production of carbon materials through sintering pot experiments. Gan and Fan et al. [14,21] conducted experiments utilizing sintering pot to investigate the impact of substituting varying proportions of coke powder with wood chips and other biomass on the quality of sintered ores and the evolution of hazardous gases in the sintered exhaust gases. Through kinetic studies on the role of biochar in pellet reduction, researchers [22-23] demonstrated that the overall reduction reaction of composite pellets is governed by reaction gas diffusion and biochar gasification. As a reducing agent, biochar exhibits higher activity, whereby its rapid volatilization initially facilitates carbon conversion and iron ore reduction. Concurrently, carbon gasification and indirect reduction reactions occur synergistically. Current research on biomass in the ironmaking field primarily focuses on the macroscopic process level, such as the substitution of coke powder with biomass in the sintering process to reduce NOx and SO_2 emissions in sintering flue gas. In blast furnace injection, the hydrogen-rich characteristics of biomass facilitate indirect reduction, but their drawbacks limit injection efficiency. However, these studies have not yet clarified the micro-scale influence of biomass on pore evolution and mineral phase changes in iron ore pellets. Particularly when biomass is used for composite iron ore balling, the interaction between its pyrolysis products and minerals directly affects pellet performance.

This study utilized waste wood chips, rice husks, bamboo, and high-silica magnetite concentrate as raw materials to prepare biomass composite pellets for blast furnaces. The basic characteristics of biomass were determined through proximate analysis, elemental analysis, and calorific value testing, while pyrolysis properties were characterized by infrared spectroscopy and comprehensive thermal analysis. The microstructure of biomass was analyzed using Fourier transform infrared spectroscopy (FTIR), SEM-EDS, and XRD, followed by an investigation into the pelletizing ability and strength of composite pellets to understand the evolution of mineral phase microstructure. This research provides theoretical support for the preparation of high-quality biomass composite pellets for blast furnace production, contributing to low-carbon green metallurgy and the strategic iron ore supply for steel enterprises.

2. Materials and experimental methods

2.1. Raw material

In this study, biomasses such as rice husk, waste wood chips and bamboo, were placed in a drying oven at 100°C for 2 h, at which temperature excess free water was removed from the biomass without significant degradation of volatile fractions and extractable compounds. The biomass feedstock and magnetite were subjected to grinding in a planetary ball mill (320 rpm) for 1 h, followed by screening to control the particle size. The percentage of iron ore concentrate powder with particle size less than 150 μm is 94.7%, and the percentage of biomass with particle size less than 150 μm is 95.3%. The magnetite concentrate used in this study was taken from a company that produces mainly magnetite, and the magnetite concentrate was placed in a drying oven at 110°C for 2 h and quantified by X-ray fluorescence (XRF) using a Bruker S8 Tiger instrument. The magnetite concentrates contained iron oxide and a range of additional compounds, which has a total iron content of 64.94%, with 26.23% of this being FeO. The remaining impurity oxides are SiO_2 (7.31%), Al_2O_3 (0.31%), CaO (0.72%), MgO (0.47%), and TiO_2 (0.02%), which are typical of iron ores. Moreover, the percentage of SiO_2 is 55.96%, Al_2O_3 is 11.73%, CaO is 4.16%, and MgO is 2.1% in the bentonite.

2.2. Experimental process and apparatus

Thermogravimetric experiments: The pyrolytic characteristics of samples were studied using a thermogravimetric analyzer (BC-S, TG-1550 model, Tianjin Baichuan Experimental Instruments). Approximately 10 mg of each feedstock was placed into a circular crucible with a height of 2 mm and a diameter of 5 mm. The crucible was then positioned in the instrument, and 99.99% pure N2 was introduced at a flow rate of 60 $ml \cdot min^{-1}$. The temperature was heated to 850°C at a rate of $10°C \cdot min^{-1}$.

Pelletizing experiment: By considering the influence of biomass physical properties and addition amount on pellet formation, as well as the effect of biomass on pellet strength during oxidative roasting. Using 4 kg of magnetite ore as the base material, biomass was added at mass ratios of 3%, 5%, and 7%, while bentonite was incorporated at a 1.5% mass ratio. Raw materials were thoroughly mixed to ensure uniform incorporation, after which the evenly mixed raw materials are sealed and allowed to stand for a period of 2 h. Qualified green pellets (10-13 mm particle size) were produced via droplet-based balling and fog-like growth using a disc pelletizer (600 mm diameter, 45° inclination, 30 rpm), with the moisture content of green pellets controlled at 7.5-8.5% of the total material mass. The green pellets were then dried in a 110°C electric thermostatic oven for 2 h to remove free water introduced during pelletizing.

Roasting Experiments: The roasting experiments were conducted in a high-temperature muffle furnace using a three-stage heating protocol to prevent pellet bursting caused by rapid temperature ramping. At room temperature, composite pellets were placed in corundum crucibles and loaded into the furnace chamber under atmospheric pressure. The three-stage preheat roasting program was as follows: heating from room temperature to 450°C at $10°C \cdot min^{-1}$, then to 925°C at $8°C \cdot min^{-1}$ (held at 925°C for 40 min), followed by heating to 1250°C at $5°C \cdot min^{-1}$ (held at 1250°C for 40 min), after which the furnace was allowed to cool naturally to room temperature. Samples were characterized to analyze their metallurgical behavior and microstructure. The process flow chart for biomass composite pellet preparation is shown in Fig. 1.

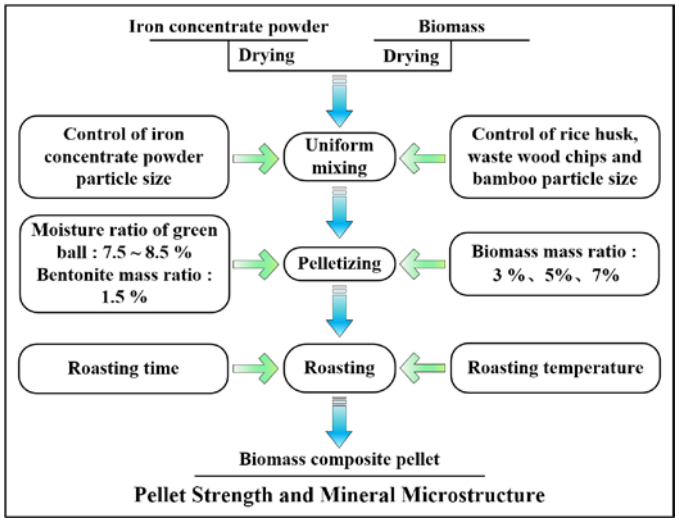

Fig. 1. Process flow chart for the preparation of biomass composite pellets using waste wood chips, rice husk, bamboo and iron ore powder

2.3. Analytical procedures

The biomass utilized in this study was analyzed using a PerkinElmer PE 2400II CHNS/O organic element analyzer for carbon, hydrogen, oxygen, nitrogen, and sulfur (C, H, O, N, S) content. Moisture, ash, volatile matter, and fixed carbon contents were determined via standard testing protocols and characterized by a Cary 630 Fourier transform infrared (FTIR) spectrometer. The main phases of the specimen powders were determined using X-ray diffraction (XRD, Bruker D8 Advance). The XRD scanning parameters were as follows: a 2θ angular range of 5-90°, a step size of 0.02°, and a scanning rate of 5 min per step. Ten pellet samples were randomly selected from the prepared qualified green pellets. Each sample was freely dropped from a height of 0.5 m onto a 10 mm thick steel plate until cracks or fragmentation occurred in the pellets. The average number of falling times for the ten pellet samples is calculated to determine the falling strength of the pellet sample. The porosity of roasted pellets was measured in accordance with the national standard (GB/T 24586-2009). The calculation formula for porosity is as follows:

$$P = \frac{\rho - \rho_a}{\rho} \times 100 \quad (1)$$

$$\rho_a = \frac{m_1}{m_3 - (m_2 - m_4)} \rho_1 \quad (2)$$

P is porosity, %; ρ is the true density, the unit is grams per cubic centimeter (g·cm^{-3}), the average of acceptable analytical values; ρ_a is the apparent density, the unit is grams per cubic centimeter (g·cm^{-3}), and the average value of the acceptable analysis value; m_1 is the mass of the sample in air, in grams (g); m_2 is the sum of the mass of the sample and the test basket water, and the unit is gram (g); m_3 is the mass in the wet bulb air, the unit is gram (g); m_4 is the mass of the water in the test basket in grams (g); ρ_1 is the density of distilled water at the test temperature in grams per cubic centimeter (g·cm^{-3}).

After water immersion to saturate the pellet pores, the sample mass in air and its mass in water of known density are separately weighed. The volume is calculated using Archimedes' principle, and the apparent density is then derived by dividing the dry pellet mass in air by this volume. For true density measurement, the sample is placed in a container of known volume, into which a defined amount of helium is introduced and sealed. The initial pressure within the container is measured by a pressure sensor, after which the gas is allowed to diffuse into another container with known pressure and volume. The equilibrium pressure in the connected containers is determined using the pressure sensor. By applying the ideal gas law, the true volume of the sample is calculated, and the true density is obtained by dividing the sample mass by this volume.

3. Results and discussion

3.1. Characterization of biomass

3.1.1. Industrial, calorific and elemental analysis of biomass

To characterize the fundamental properties of the biomass, proximate, elemental, and calorific value analyses were conducted, with results tabulated in TABLE 1. TABLE 1 reveals that all three biomasses exhibit low sulfur (≤0.115 wt.%) and nitrogen (≤0.73 wt.%), significantly lower than those of coke (e.g., 0.5-2.0 wt.% S, [24]) and anthracite (e.g., 1.0-1.5 wt.% S, [25]). This highlights biomass as a promising energy alternative for reducing SO_x and NO_x emissions, thereby alleviating environmental impacts. In addition, the C and H content of biomass has a great influence on the improvement of its own combustion performance, the C and H content of rice husk and bamboo is lower than

TABLE 1

Proximate and ultimate analyses of the biomass

Biomass type	Rice husk	Waste wood chips	Bamboo
Proximate analysis (wt.%, air dried)			
Moisture, M	0.72	0.60	0.34
Ash, A	21.93	4.75	17.07
Volatile matter, V	63.99	77.64	68.27
Fixed carbon, FC	13.36	17.01	14.32
Ultimate analysis (wt.%, dry ash)			
Carbon, C	29.00	43.96	35.39
Hydrogen, H	3.538	5.356	4.634
Oxygen, O	33.605	44.302	36.626
Nitrogen, N	0.73	0.30	0.73
Sulfur, S	0.115	0.082	0.103
High calorific value (MJ·kg^{-1})	13.38	18.37	16.23
Component analysis (wt.%, air dried)			
Cellulose	34.26	42.36	42.55
Hemicellulose	24.55	29.67	24.95
Lignin	21.68	23.15	27.49
Extract	19.51	4.82	5.01

that of waste wood chips, while the volatile fraction (77.64%) and fixed carbon (17.01%) of waste wood chips are higher than those of rice husk (63.99%, 13.36%) and bamboo (68.27%, 14.32%), and their ash content (4.75%) is much lower than that of rice husk (21.93%) and bamboo (17.07%). Ash affects the heat transfer rate and the content of agglomeration products during pyrolysis [26], and higher volatile and fixed carbon and lower ash are beneficial for the combustion performance of raw materials [27-28].

3.1.2. Thermogravimetric and infrared spectroscopic analysis of biomass

The hydrophilicity and cohesiveness of biomass directly affect pellet formation. Therefore, SEM detection and analysis were conducted on the microstructure of biomass. Fig. 2(a) and Fig. 2(b) in the photograph represent micrographs of waste wood chips particles and waste wood chips cross-sectional surfaces, respectively. It can be seen from Fig. 2(a) that the surface of waste wood chips is rougher and intricate. There are holes in the fibers arranged in the same growth direction and uniform size, forming thin strips, as shown in Fig. 2(b). There are hydrogen bonds between cellulose molecules, which produce certain toughness. As shown in Fig. 2(c) and Fig. 2(d) respectively represent the micrographs of rice husk particles and cross section of rice husk. It can be seen from Fig. 2(c) that the surface of rice husk is rough like scales with holes. The outer layer is smoother than the inner layer. Fig. 2(e) and Fig. 2(f) in the photograph represent micrographs of bamboo grains and cross sections, respectively. As can be seen from Fig. 2(e), the shape of bamboo particles varies greatly in different parts. Bamboo fibers are piled up into vascular bundles and parenchyma cells form bamboo walls, which is caused by the different number, strength and arrangement of bamboo fibers in different parts of bamboo. The outer surface is obviously protruding and evenly distributed in the same direction, while the inner surface is clumped together and rough. It can be seen from Fig. 4(b) that the vascular bundle formed by the accumulation of bamboo fibers is obviously distributed in a filamentous manner.

With increasing temperature, water loss and volatilization of cellulose, hemicellulose and lignin by pyrolysis are the main contributors to biomass weight loss. However, depending on the type of biomass, the characteristics of the pyrolysis process can also vary. It is clear from the TG curves in Fig. 3(a), Fig. 3(b) and Fig. 3(c) that herbaceous biomass has a broader weight loss curve than woody biomass and that there are three main stages of biomass mass loss. The first stage occurs before 100°C and is dominated by water loss, when the temperature rises and water has been removed from all three biomasses, a weight loss of about 4.5%. The second phase takes place between 100°C and 400°C. The analysis shows that cellulose, hemicellulose and lignin are the main substances that undergo pyrolysis in biomass [29-32]. The pyrolysis behavior of cellulose mainly occurs between 300°C and 400°C, and that of hemicellulose mainly occurs between 215°C and 325°C. Although the pyrolysis behavior of lignin occurs after 200°C, the fastest pyrolysis rate occurs between 310°C and 410°C [33]. The third stage is after 400°C, where the three biomasses still show a weight loss behavior at the end of the pyrolysis cycle, resulting from the pyrolysis of residual lignin, biomass char and other inorganic matter.

The DTG curves in Fig. 3(a), Fig. 3(b) and Fig. 3(c) show that for all three samples the initial mass loss is complete before 100°C.

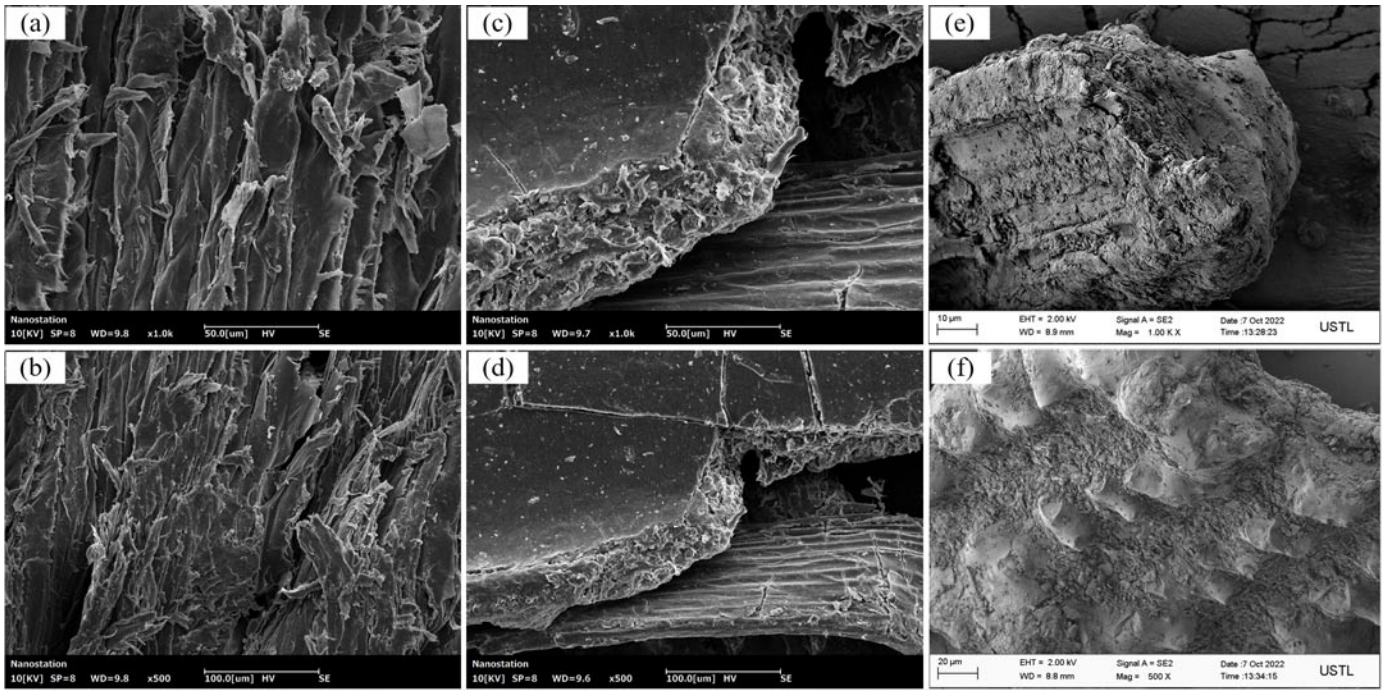

Fig. 2. Analysis of SEM images of biomass: (a) SEM image of the waste wood chips cross-section, (b) SEM image of waste wood chips particles, (c) SEM image of the rice husk cross-section, (d) SEM image of rice husk particles, (e) SEM image of the bamboo cross-section, (f) SEM image of bamboo particles

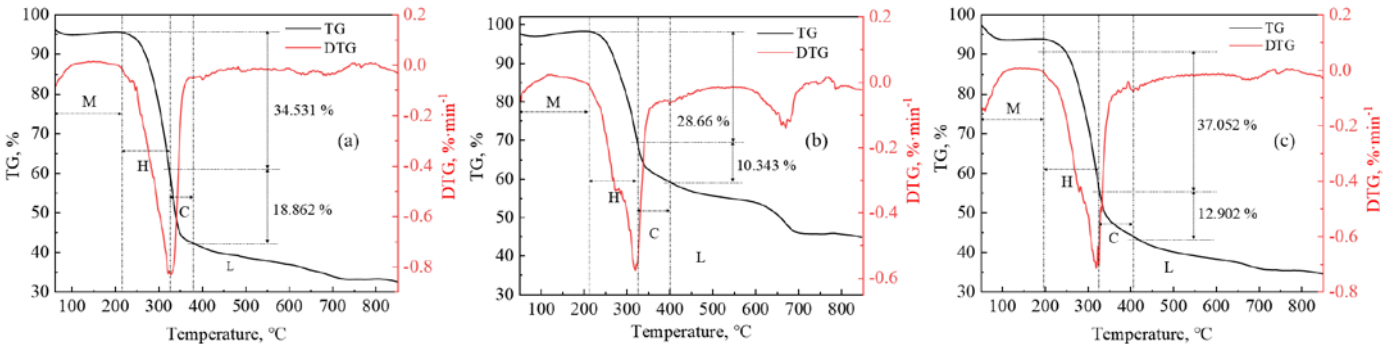

Fig. 3. Thermogravimetric analysis of biomass: (a) Thermogravimetric (TG-DTG) curves of waste wood chips, (b) Thermogravimetric (TG-DTG) curves of rice husks, (c) Thermogravimetric (TG-DTG) curves of bamboo (M: moisture, H: hemicellulose, C: cellulose, L: lignin)

This corresponds to the loss of moisture. The most pronounced peak in weight loss rate for the three biomasses occurred at around 320°C. The loss of mass of the samples varied with increasing temperature, the most pronounced being bamboo with a decrease of 37.052%. The TG-DTG curve intersection method was used to determine the pyrolysis temperature of the three biomasses, which was in the range of 270~350°C. As shown in Fig. 3(c), a pronounced peak appears on the TG-DTA curve of rice husk biomasses in the range of 650~700°C. This is because after the loss of volatile compounds in rice husk biomass, some persistent intermediate products (such as aromatic compounds) begin to decompose, which are more stable and have internal structures of lignin and cellulose. The concentration of these persistent intermediate products accumulation with the increase in pyrolysis temperature, and decomposition occurs when the temperature rises to a certain level. Large amounts of volatile fractions containing the elements C, H and O, including CO, H_2 and CH_4, were produced by the thermal decomposition of cellulose, hemicellulose and lignin. The pyrolysis of waste wood chips and bamboo was completed at about 500°C, and the weight was reduced by 50%.

The FTIR spectra in Fig. 4(a), Fig. 4(b) and Fig. 4(c) shows the functional group changes of the three biomasses at different temperatures at 10°C·min^{-1} heating rate. It can be clearly seen that the peaks of the woody biomass samples at 3430 cm^{-1} (OH stretching), 2920-2930 cm^{-1} (CH_3 and CH_2 stretching), 1619-1570 cm^{-1}, 1458-1510 cm^{-1} (Benzene ring vibration), 1400-1440 cm^{-1} (OH in plane bending, CH deformation), 1360-1380 cm^{-1} (CH vibration) decrease after 300°C. Thermal decomposition of cellulose, hemicellulose and lignin is responsible for all these phenomena. Thermogravimetric analysis shows that the pyrolysis of biomass starts at 200°C with the decomposition of hemicellulose and lignin. This reduces the peaks of hydroxyl, benzene, methyl and methylene groups [34-35]. TABLE 2 lists all of the possible vibrations in the spectra obtained from the synchrotron IR studies [35,33]. Furthermore, the oscillation (C=O stretching of aldehydes and esters) of woody biomass is significantly weaker at 1740 cm^{-1} after 200°C. The vibrations at 1690 cm^{-1} (C=O stretching of carboxylic acids) at 300°C and 400°C are produced by the volatile carboxylic acids formed during pyrolysis. Lignin caused shaking at 1220 cm^{-1} and 1270 cm^{-1}, and the peak began to weaken at 200°C for waste wood chips and bamboo biomass, but the weakening trend was not evident for rice husks. Because lignin is amorphous, it is unstable and therefore thermally unstable, which causes woody biomass to pyrolyze faster. It is important to select the right biomass as an additive because the biomass has a greater ability to influence the pyrolysis rate due to differences in cellulose and lignin content.

3.2. Pelletization results

During the whole pelletizing process, the pelletizing performance will decrease with the increase of biomass content. In line with the principle of “drip into ball, mist growth”, the water

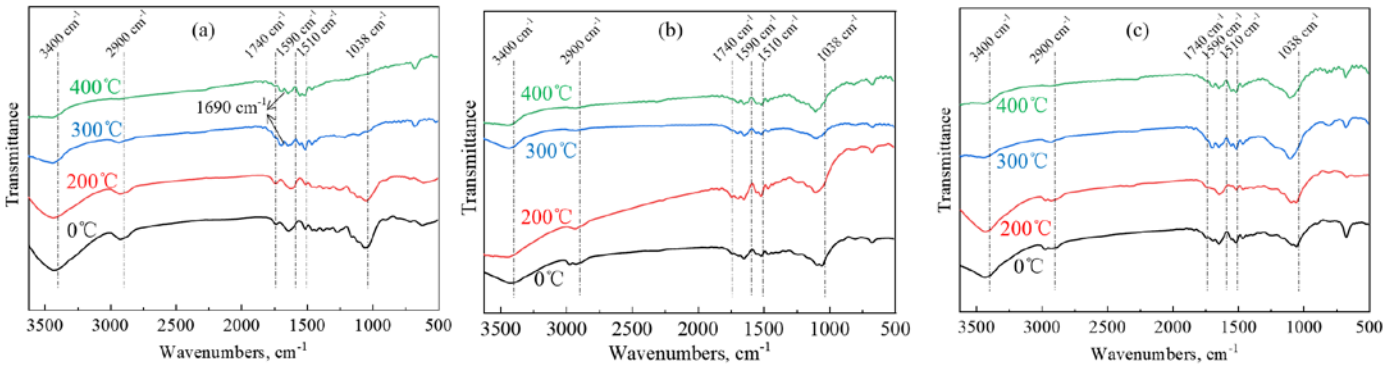

Fig. 4. Infrared analysis of biomass: (d) Fourier transform infrared (FTIR) spectra of products from waste wood chips treated at different temperatures, (d) Fourier transform infrared (FTIR) spectra of products from rice husks treated at different temperatures, Fourier transform infrared (FTIR) spectra of products from bamboo treated at different temperature

TABLE 2

Peak assignment for in-situ synchrotron IR study

Scrap wood chips	Rice husk	Bamboo	Functional group assignment
Wavenumber, cm^{-1}	Wavenumber, cm^{-1}	Wavenumber, cm^{-1}	
3436	3432	3434	OH stretching
2922	2931	2930	CH symmetric and anti-symmetric stretching
1741-1690	1795-1699	1747-1699	C=O stretch
1619-1556	1619-1572	1619-1573	Aromatic ring stretch + C=O stretch
1507-1458	1508-1472	1509-1492	Aromatic ring stretch
1472-1458	1472-1455	1473-1455	CH_2 scissors vibration
1433-1397	1420-1395	1420-1396	OH in plane bending, CH deformation
1433 (at 300°C and 400°C)			C-O-H in plane bending
1375	1359	1377	CH vibration
1269	1281	1260	C-O stretch (of guaiacyl ring)
1236	1239	1216	C-O stretch (of guaiacyl ring)
1160	1146	1152	C-O-C stretch
1036	1054	1050	C-O stretch, C-H of guaiacyl ring
100-600			=C-H out of plane bending

distribution technology in the disc has a certain influence on the size growth of raw ball. The pellets size formed cue ball growing rapidly within 1 minute, and the water distribution rate was timely controlled. The pellets grew evenly with little fluctuation. The pellets size reached the qualified size (10~13 mm) at 17 min. When the proportion of biomass increases, the growth process of cue ball will fluctuate obviously, among the three kinds of biomass, bamboo has the most obvious performance, followed by rice husk. At the same time, it was found that the material added with waste wood chips had stronger hydrophilicity, and the fiber structure of waste wood chips was conducive to the increase of material bonding in the pelletizing process. In addition, the pellets size is faster before 5 mm, and then the change of pellets size requires further control of the water distribution rate and the rate of adding materials to solve the problem of uneven growth.

The compressive strength of composite pellets refers to the maximum crushing load applied by external pressure, and testing the compressive strength of composite pellets characterizes their mechanical strength. In the pellet production process, factors such as water content, wettability of binders (e.g., bentonite), porosity of finished pellets, microstructure, and gangue components collectively influence the strength of iron ore pellets. Additionally, apart from the influence of raw material properties, pellet strength is closely related to roasting time, roasting temperature, heating rate, and roasting atmosphere. The study varied the proportion of biomass while keeping other conditions constant to further investigate the effect of biomass on pellet strength and structure.

3.2.1. Effect of waste wood chips on composite pellets

As shown in Fig. 5, the falling strength of waste wood chip composite pellets showed an upward trend with increasing biomass content. When the wood chip proportion was 7%, the number of drops per composite pellet reached a maximum of 3.9 times/pellet. Meanwhile, the compressive strength of waste wood chip green pellets significantly decreased, reaching a maximum of 10.94 $N \cdot P^{-1}$ at 3% biomass addition, then decreasing sequentially. However, when the waste wood chip content reached the maximum addition of 7%, the compressive strength of green pellets still exceeded that of the control group. After roasting, the compressive strength of biomass composite roasted pellets generally increased with increasing biomass content, exceeding 2414.72 $N \cdot P^{-1}$. For long-distance transportation, the compressive strength of pellets should reach 2500.00 $N \cdot P^{-1}$, while for direct use in blast furnace ironmaking, it can be appropriately reduced to not less than 2000.00 $N \cdot P^{-1}$. When the biomass content of waste wood chips was 7%, the maximum compressive strength of pellets reached 2660.03 $N \cdot P^{-1}$, meeting the requirements. As biomass content increased from 0% to 7%, the pellet porosity gradually increased, reaching a maximum of 45.47% when the waste wood chip proportion was 7%.

Figs. 6(a) and 6(b) show the microstructures of the interior and surface of roasted pellets, respectively, while Fig. 6(c) presents X-ray diffraction (XRD) patterns of biomass composite pellets with different waste wood chip proportions after roasting. XRD analysis indicates the presence of minor $2FeO \cdot SiO_2$ and residual carbon in waste wood chip composite pellets, with peak intensities increasing with biomass content. SiO_2 peaks are primarily centered at approximately 20.833° and 26.621°, while residual carbon peaks in biomass mainly cluster at 26.621° and 43.521°. In the cross-section of roasted pellets, flocculent substances around pores are clearly observable, which were identified as bridging solid solutions formed by SiO_2 and Fe_2O_3 during high-temperature roasting. Further observation of the pellet surface reveals interconnected phases between massive particles around surface pores, which are inferred to be minor complex silicate structures with blocking property based on EDS data. The formation of distinct flocculent or blocking property structures between pores and raw material particles during roasting plays a positive role in the consolidation of biomass composite pellets.

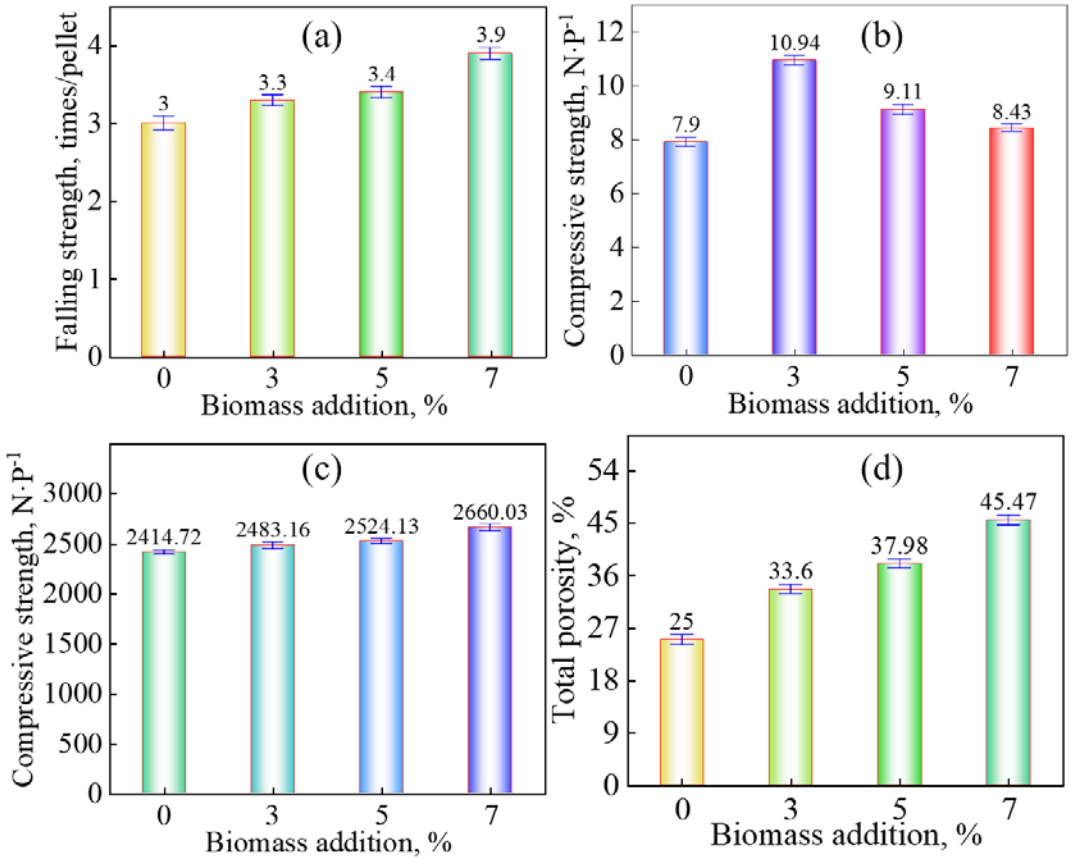

Fig. 5. Strength of composite pellets of waste wood chips: (a) Falling strength of green pellets; (b) Compressive strength of green pellets; (c) Compressive strength of finished pellets; (d) Total porosity of finished pellets

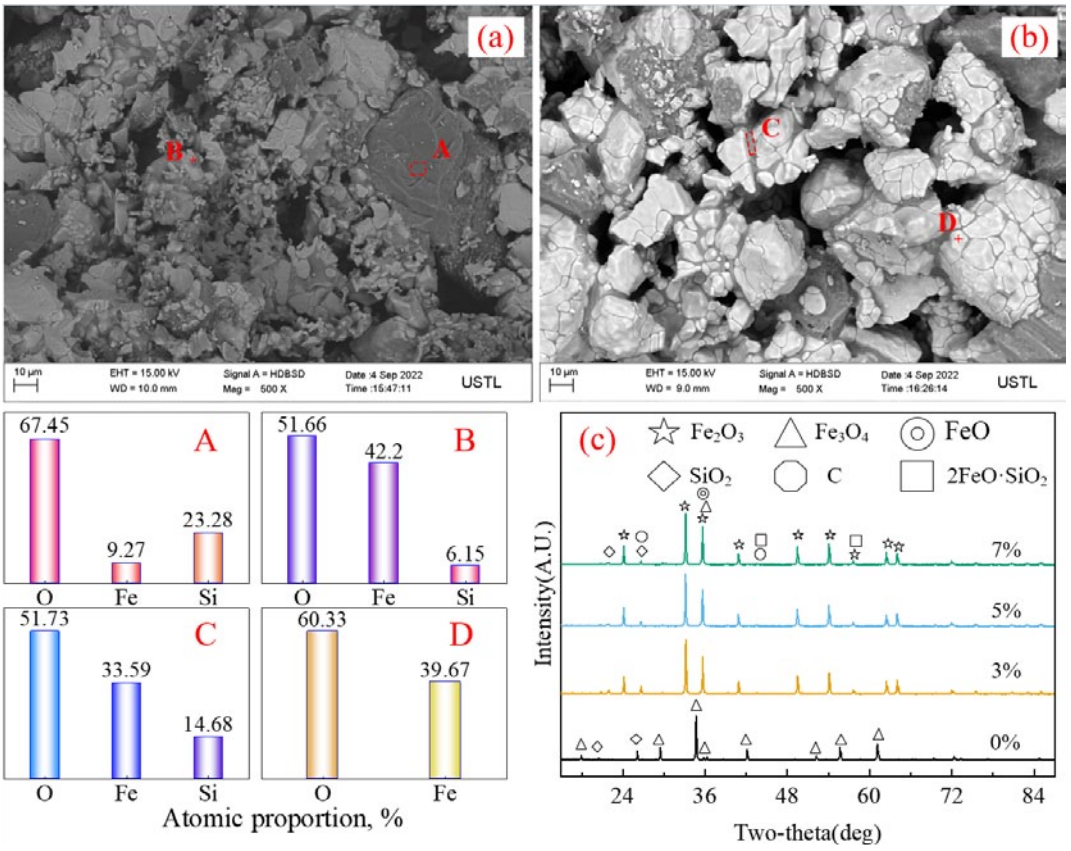

Fig. 6. Composite pellets of waste wood chips: (a) SEM analysis of internal of finished pellets; (b) SEM analysis of the surface of finished pellets; (c) XRD pattern of finished pellets

3.2.2. Effect of rice husk on composite pellets

As the biomass ratio was increased, falling strength of rice hull composite pelletizing was not significantly altered, and the increase in strength was not evident compared to the contrast pelletizing (as showed in Fig. 7). The compressive strength of rice husk composite green pellets showed an upward trend. When the rice husk proportion increased to 5%, the strength exceeded that of the control group green pellets. At 7% addition, the compressive strength of rice husk composite green pellets reached a maximum of 8.92 $N \cdot P^{-1}$. After roasting the pellets with the increase of biomass the overall pellet strength of rice husk showed an increasing trend, the pellet strength of rice husk roasted pellets was above 2200.00 $N \cdot P^{-1}$ when the biomass content reached 7%, reaching 2264.39 $N \cdot P^{-1}$, but lower than the comparison pellet strength (2414.72 $N \cdot P^{-1}$). Add 3% ~ 4% of coke powder to the raw materials to produce porous pellets with a porosity of 30% ~ 40%. Adding 2% of High marsh peat with a particle size smaller than 0.5mm to the granular material can also increase the porosity of the pellets by 8% ~ 10%. When the proportion of rice husk biomass is increased to 7%, the porosity of the composite pellets reaches 38.88%, higher than that of regular pellets (20% ~ 30%).

SEM-EDS analysis of the interior and surface of rice husk composite pellets, as shown in Figs. 8(a) and 8(b), clearly revealed that the particle surface exhibited solid solutions of various shapes and sizes, which were irregularly wrapped around the particle surface. At point B, particles were observed to be interconnected but not tightly bonded, and EDS analysis showed that the atomic ratio of Fe to O was close to that of Fe_3O_4. This preliminarily indicates that location B is Fe_3O_4, confirming that the presence of biomass may have prevented the complete oxidation of Fe_3O_4 around pellet pores. Elemental analysis at point A showed that the precipitate was $2FeO \cdot SiO_2$.

3.2.3. Effect of bamboo on composite pellets

From the Fig. 9, the overall strength of bamboo biomass composite pellet was unsatisfactory, the drop strength of raw composite pellets and the compressive strength of roasted pellets were lower than the comparison pellets, only the compressive strength of raw pellets when biomass was added to 3% was higher than the comparison pellets. Figs. 10(a) and (b) show the internal and surface microstructures of bamboo composite pellets, respectively. SEM images clearly reveal that particles around pores are smaller, loosely connected by the liquid phase, and lack the structural integrity and flocculent structures observed in waste wood chip composite pellets. Liquid-phase connections between small particles within the pellets were also observed, presumably $2FeO \cdot SiO_2$. The formation of the liquid phase serves a bridging role, and appropriate filling of liquid phase into pores can enhance the overall strength of pellets. As shown in Fig. 9(c), the compressive strength of bamboo composite pellets was lowest at a 5% bamboo addition. Qualitative XRD analysis confirmed

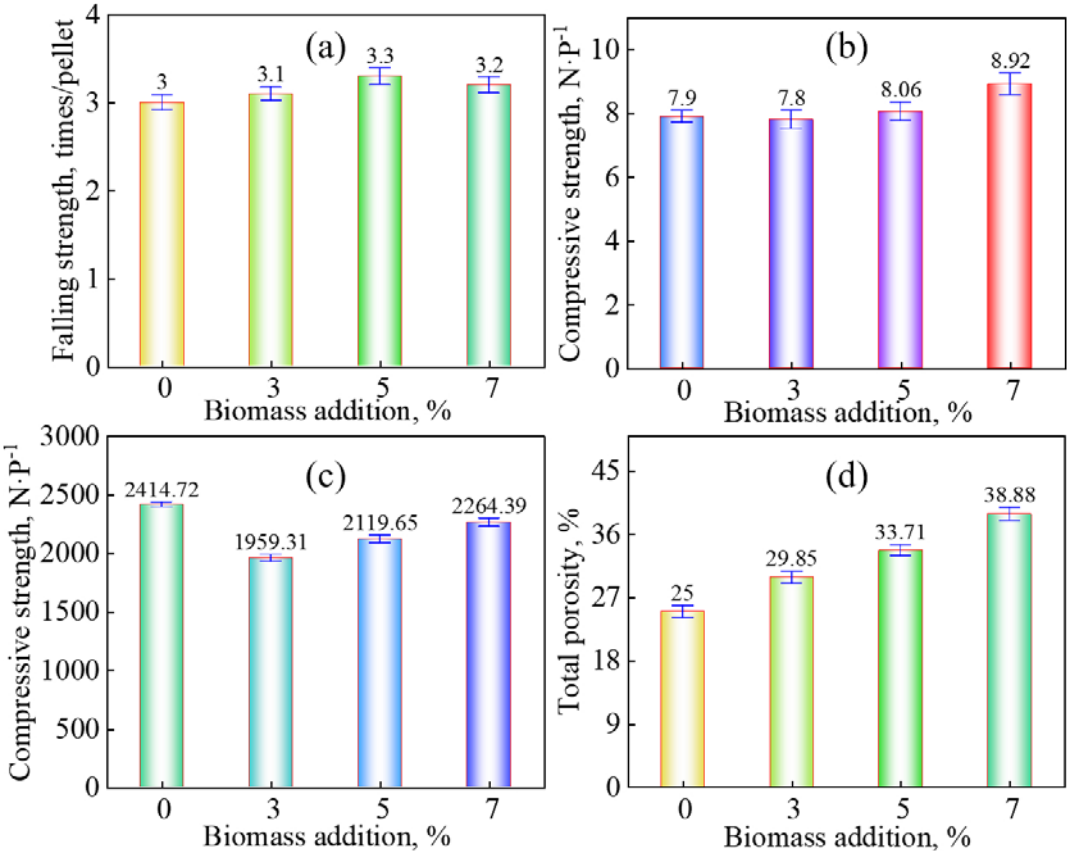

Fig. 7. Strength of rice husk composite pellets: (a) Falling strength of green pellets; (b) Compressive strength of green pellets; (c) Compressive strength of finished pellets; (d) Total porosity of finished pellets

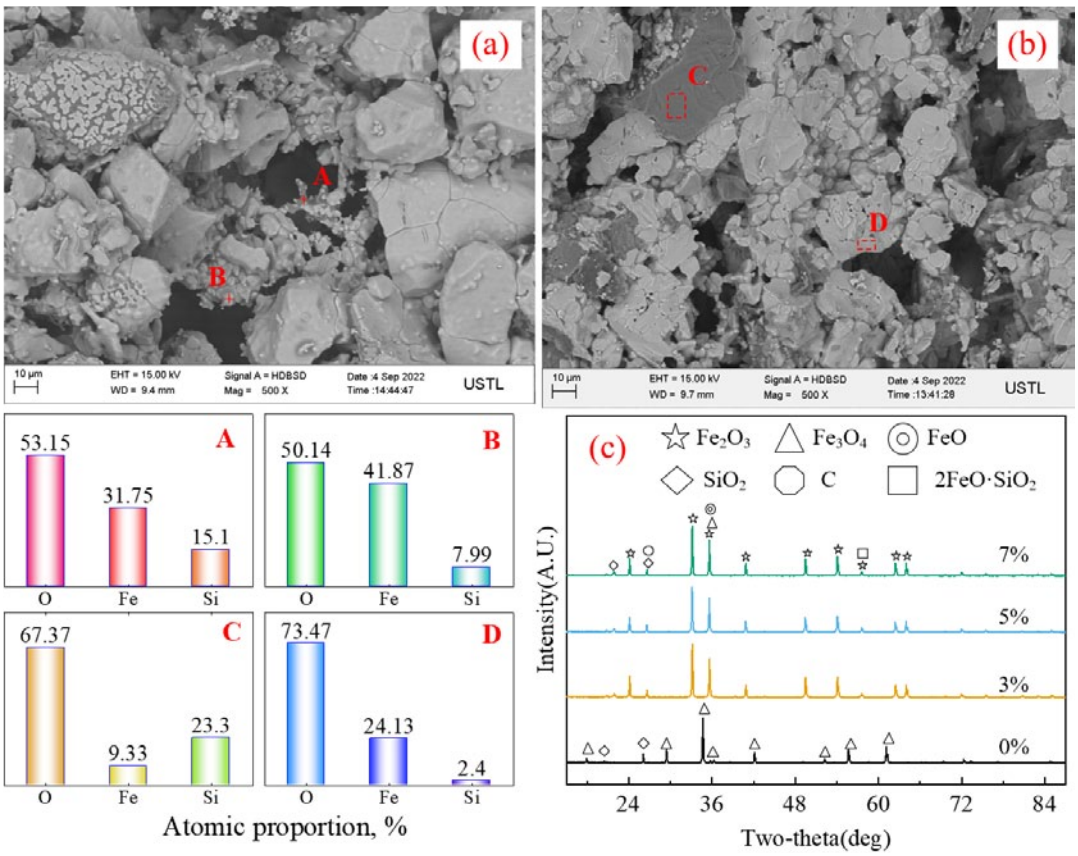

Fig. 8. Rice husk composite pellets: (a) SEM analysis of internal of finished pellets; (b) SEM analysis of the surface of finished pellets; (c) XRD pattern of finished pellets

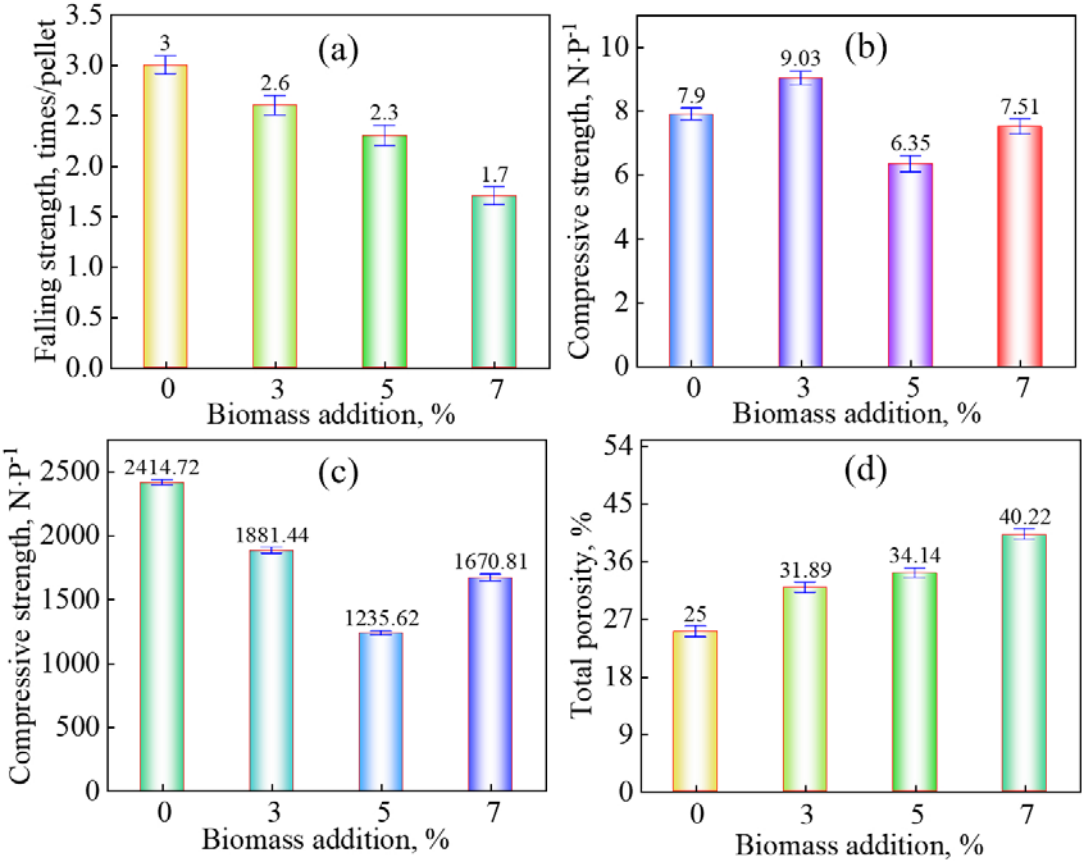

Fig. 9. Strength of bamboo composite pellets: (a) Falling strength of green pellets; (b) Compressive strength of green pellets; (c) Compressive strength of finished pellets; (d) Total porosity of finished pellets

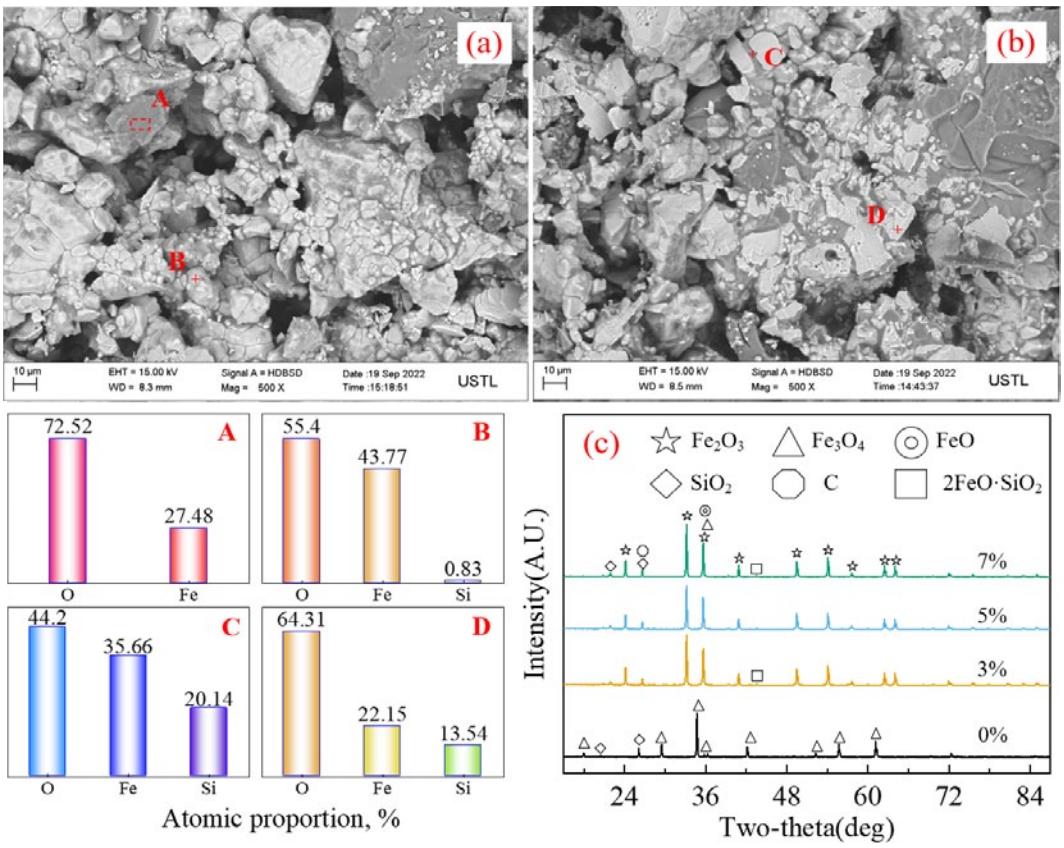

Fig. 10. Bamboo composite pellets: (a) SEM analysis of internal of finished pellets; (b) SEM analysis of the surface of finished pellets; (c) XRD pattern of finished pellets

the presence of $2FeO{\cdot}SiO_2$ in composite pellets with 3% and 7% bamboo additions, where liquid-phase filling in pores contributed to strength enhancement. This is consistent with previous findings, and when the bamboo addition reached 7%, the pellet porosity reached 40.22%. The cellulose and hemicellulose contents in the biomass are directly proportional to the volatile content of the biomass, and the volatile content of the biomass is directly proportional to the porosity of the composite pellets, the porosity determines the microstructure of the biomass composite pellets.

3.3. Roasting reaction process of biomass composite pellets

Through the analysis of biomass properties and the effect of biomass on the strength and microstructure of composite pellets, the roasting reaction mechanism of biomass composite pellets was further derived, as shown in Fig. 11. Biomass has a lower reaction temperature than ores and higher volatile content, so during the initial roasting stage of biomass composite pellets, the biomass in the composite pellets first undergoes pyrolysis. The thermal decomposition of cellulose, hemicellulose, and lignin in biomass produces a large amount of reducing gases containing carbon, hydrogen, and oxygen, mainly composed of CO_2, CO, H_2, and CH_4, creating a local anoxic or reducing gas environment [36-37]. Thus, Fe_3O_4 is not fully oxidized to Fe_2O_3 during roasting. The residual carbon generated by biomass, together with reducing gases, forms a local reducing atmosphere around the pores, promoting the prereduction reaction of particles and forming minor reduction products. Meanwhile, the generated biomass char and CO_2 further react to produce CO, facilitating indirect reduction. The presence of biomass not only creates gas channels from volatile release within composite pellets but also induces abundant pores due to its participation in pyrolysis, accelerating the transition from solid-solid to gas-solid reactions and promoting thermal radiation transfer into the pellet interior. This provides favorable thermodynamic and kinetic conditions for biomass composite pellets. Therefore, adding appropriate biomass to iron ore pellets can not only improve pellet quality but also contribute to energy conservation and environmental protection.

4. Conclusions

All three types of biomasses exhibited low sulfur and nitrogen contents. Waste wood chips showed the optimal contents of C, H, O elements, ash, volatile matter, and fixed carbon, along with the highest calorific value. When pyrolyzed below 500°C, waste wood chips and bamboo showed mass loss up to 50%. The peak intensity variation of rice husks in the range of 1500 to 500 cm^{-1} was opposite to that of waste wood chips and bamboo. Hydrophilicity of biomass directly influenced the pellet ability of composite pellets, with waste wood chips exhibiting the strongest hydrophilicity during pelletizing, thus leading to the highest balling rate for waste wood chip composite pellets. Strength

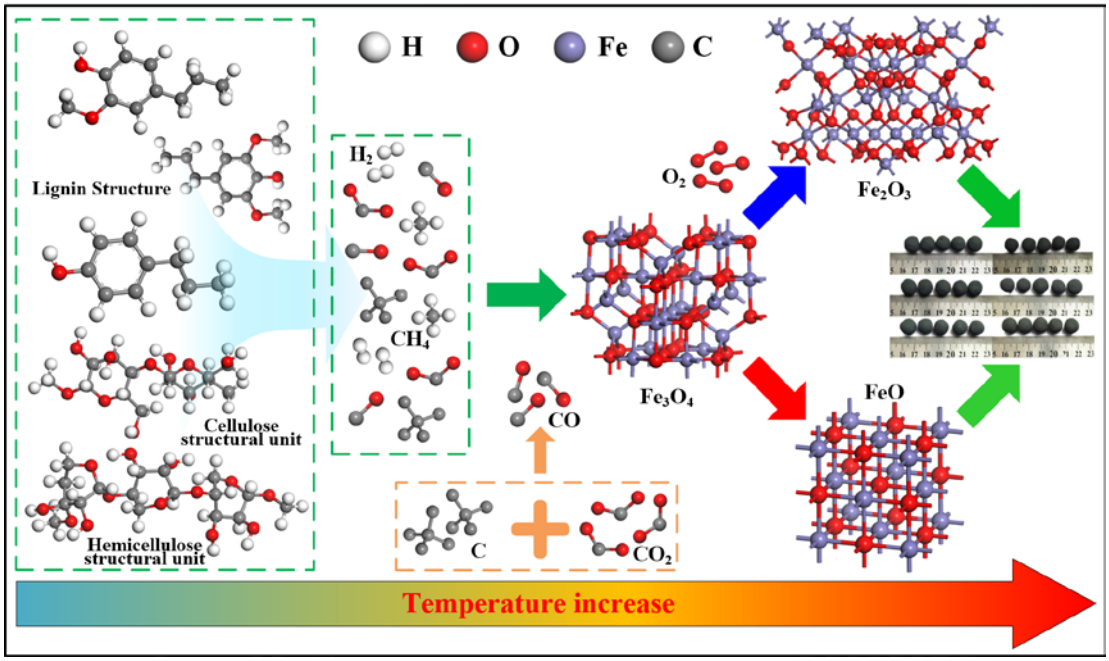

Fig. 11. Roasting reaction mechanism of biomass composite pellets

performance evaluation of biomass composite pellets showed that waste wood chip composite pellets had the best strength properties, with compressive strength reaching 2660.03 $N \cdot P^{-1}$ when the waste wood chip proportion increased to 7%.

During roasting, biomass addition increased the porosity of pellets and further created a weak hypoxic or reducing atmosphere between pellet particles. Pores and gas channels generated by biomass accelerated the diffusion of reactive gases into the pellet interior, promoting the transition from solid-solid to gas-solid reactions and improving the overall reaction state of composite pellets. Incompletely oxidized magnetite was reduced by volatile matter and biomass char generated from biomass, exhibiting local prereduction. Meanwhile, the use of high-silica magnetite formed a binding liquid phase that filled into pores, enhancing the comprehensive strength of pellets. Thus, biomass incorporation into pellets not only maintained pellet strength but also achieved a prereduction effect.

Acknowledgements

The authors received financial support from the National Natural Science Foundation of China (52104332, 52374339, 52474359), Doctoral Research Foundation of Liaoning Province, China (2023-BS-171), and The project of China Baowu Low Carbon Metallurgy Innovation Foundation (BWLCF202308).

REFERENCES

[1] N. Thibanyane, P. Agachi, G. Danha, Effects of biomass/ coal copyrolysis parameters on the product yield: A review. Procedia. Manuf. **35**, 477-487 (2019).
DOI: https://doi.org/10.1016/j.promfg.2019.07.007

[2] R.F. Wei, H.M. Li, Y.F. Lin, et al, Reduction Characteristics of Iron Oxide by the Hemicellulose, Cellulose, and Lignin Components of Biomass. Energ. Fuel. **34** (7), 8332-8339 (2020).
DOI: https://doi.org/10.1021/acs.energyfuels.0c00377

[3] N.S.K. Baharin, V.C. Koesoemadinata, S. Nakamura, et al., Conversion and characterization of Bio-Coke from abundant biomass waste in Malaysia. Renew. Energ. **162**, 1017-1025 (2020).
DOI: https://doi.org/10.1016/j.renene.2020.08.083

[4] J.L. Xu, M. Huang, Z.Y. Hu, Prediction and modeling of the basic properties of biomass after torrefaction pretreatment. J. Anal. Appl. Pyrol. **159**, 105287 (2021).
DOI: https://doi.org/10.1016/j.jaap.2021.105287

[5] G.W. Wang, J.L. Zhang, J.Y. Lee, et al., Hydrothermal carbonization of maize straw for hydrochar production and its injection for blast furnace. Appl. Energ. **266**, 114818 (2020).
DOI: https://doi.org/10.1016/j.apenergy.2020.114818

[6] X.L. Lu, X.Q. Ma, X.F. Chen, et al., Co-hydrothermal carbonization of polyvinyl chloride and corncob for clean solid fuel production-ScienceDirect. Bioresource. Technol. **301**, 1-8 (2020).
DOI: https://doi.org/10.1016/j.biortech.2020.122763

[7] M. Mayyas, R.K. Nekouei, V. Sahajwalla, Valorization of lignin biomass as a carbon feedstock in steel industry: Iron oxide reduction, steel carburizing and slag foaming. J. Clean. Prod. **219**, 971-980 (2019). DOI: https://doi.org/10.1016/j.jclepro.2019.02.114

[8] D. Khasraw, S. Spooner, H. Hage, et al., Devolatilisation characteristics of coal and biomass with respect to temperature and heating rate for HIsarna alternative ironmaking process. Fuel **284**, 119101 (2020).
DOI: https://doi.org/10.1016/j.fuel.2020.119101

[9] Q.V. Bach, T.N. Trinh, K.Q. Tran, et al., Pyrolysis characteristics and kinetics of biomass torrefied in various atmospheres. Energ. Convers. Manage. **141**, 72-78 (2017).
DOI: https://doi.org/10.1016/j.enconman.2016.04.097

[10] G. Jha, S. Soren, K.D. Mehta, Partial substitution of coke breeze with biomass and charcoal in metallurgical sintering. Fuel **278**, 118350 (2020). DOI: https://doi.org/10.1016/j.fuel.2020.118350

[11] S. Suman, et al., Substitution of coking coal with biochar for thermal and metallurgical utilization. Int. J. Sustain. Energy **41** (11), 1778-1794 (2022). DOI: https://doi.org/10.1080/14786451.2022.2110100

[12] T. Kawaguchi, M. Hara, Utilization of bomass for iron ore sintering, ISIJ. Int. **53** (9), 1599-1606 (2013). DOI: https://doi.org/10.2355/isijinternational.53.1599

[13] D.F. Chen, X.Y. Hu, X.J. Li, Biomass resource's application in iron and steel enterprises of China. Res. Iron. Steel. **43**, 60-62 (2015). DOI: https://doi.org/10.1016/j.rser.2016.07.061

[14] M. Gan, X. Fan, X. Chen, et al., Reduction of pollutant emission in iron ore sintering process by applying biomass fuels. ISIJ. Int. **52**, 9, 1574-1578 (2012). DOI: https://doi.org/10.2355/isijinternational.52.1574

[15] H. Suopajärvi, E. Pongrácz, T. Fabritius, Bioreducer use in Finnish blast furnace ironmaking – Analysis of CO_2 emission reduction potential and mitigation cost. Appl. Energ. **124**, 82-93 (2014). DOI: https://doi.org/10.1016/j.apenergy.2014.03.008

[16] D. Cholico-Gonzalez, N.O. Lara, M.A.S. Miranda, et al., Efficient metallization of magnetite concentrate by reduction with agave bagasse as a source of reducing agents. Int. J. Min. Met. Mater. **28** (4), 603-611 (2021).

[17] D.B. Guo, B.H. Cui, Z.H. Chen, Biomass enhances the reduction of oxidized pellets with carbon monoxide. Bioresour. Technol. **331**, 124973 (2021). DOI: https://doi.org/10.1016/j.biortech.2021.124973

[18] R. Wei, D. Cang, Y. Bai, D. Huang, X. Liu, Reduction characteristics and kinetics of iron oxide by carbon in biomass. Ironmak. Steelmak. **43** (2), 144-152 (2016). DOI: https://doi.org/10.1179/1743281215y.0000000061

[19] T.C. Ooi, E. Aries, B.C.R. Ewan, et al., The study of sunflower seed husks as a fuel in the iron ore sintering process. Miner. Eng. **21** (2), 167-177 (2008). DOI: https://doi.org/10.1016/j.mineng.2007.09.005

[20] X. Fan, Z. Ji, M. Gan, et al., Integrated assessment on the characteristics of straw-based fuels and their effects on iron ore sintering performance. Fuel. Process. Technol. **150**, 1-9 (2016). DOI: https://doi.org/10.1016/j.fuproc.2016.05.022

[21] S.A. Kumar, S.O. Prakash, S.R, Reduction Behavior and Kinetics of Iron Ore-Charcoal Composite Pellets for Sustainable Ironmaking. Metall. Mater. Trans. B. **54** (2), 823-832 (2023). DOI: https://doi.org/10.1007/s11663-024-03083-5

[22] Q. Hu, D.D. Yao, Y.P. Xie, et al., Study on intrinsic reaction behavior and kinetics during reduction of iron ore pellets by utilization of biochar. Energ. Convers. Manage. **158**, 1-8 (2018). DOI: https://doi.org/10.1016/j.enconman.2017.12.037

[23] L. Lu, M. Adam, M. Kilburn, et al., Substitution of Charcoal for Coke Breeze in Iron Ore Sintering. ISIJ. Int. **53** (9), 1607-1616 (2013). DOI: https://doi.org/10.2355/isijinternational.53.1607

[24] S. Ceylan, Y. Topcu, Z. Ceylan, Thermal behaviour and kinetics of alga Polysiphonia elongata biomass during pyrolysis. Bioresource. Technol. **171**, 193-198 (2014). DOI: https://doi.org/10.1016/j.biortech.2014.08.064

[25] L. Sanchez-Silva, D. Lopez-Gonzalez, J. Villasenor, et al., Thermogravimetric-mass spectrometric analysis of lignocellulosic and marine biomass pyrolysis. Bioresource. Technol. **109**, 163-172 (2012). DOI: https://doi.org/10.1016/j.biortech.2012.01.001

[26] S.V. Vassilev, D. Baxter, L.K. Andersen, et al., An overview of the chemical composition of biomass. Fuel **89** (5), 913-933 (2010). DOI: https://doi.org/10.1016/j.fuel.2009.10.022

[27] T. Kan, V. Strezov, T.J. Evans, Lignocellulosic biomass pyrolysis: A review of product properties and effects of pyrolysis parameters. Renew. Sust. Energ. Rev. **57**, 1126-1140 (2016). DOI: https://doi.org/10.1016/j.rser.2015.12.185

[28] X.F. Sun, R.C. Sun, P. Fowler, M.S. Baird, Extraction and Characterization of Original Lignin and Hemicelluloses from Wheat Straw. J. Agr. Food. Chem. **53** (4), 860-870 (2005). DOI: https://doi.org/10.1021/jf040456q

[29] W.F. Cai, Z.Y. Luo, J.S. Zhou, Q.H. Wang, A review on the selection of raw materials and reactors for biomass fast pyrolysis in China. Fuel Process. Technol. **221**, 106919 (2021). DOI: https://doi.org/10.1016/j.fuproc.2021.106919

[30] Y.F. Cai, Z.H. Zheng, et al., A review about pretreatment of lignocellulosic biomass in anaerobic digestion: achievement and challenge in Germany and China. J. Clean. Prod. **299**, 126885 (2021). DOI: https://doi.org/10.1016/j.jclepro.2021.126885

[31] A. Elgarahy, A. Hammad, D.M. El-Sherif, et al. Thermochemical conversion strategies of biomass to biofuels, techno-economic and bibliometric analysis: A conceptual review. J. Environ. Chem. Eng. **9**, 6, 106503 (2021). DOI: https://doi.org/10.1016/j.jece.2021.106503

[32] G.W. Xu, D.R. Bai, C.M. Xu, M.Y. He, Challenges and opportunities for engineering thermochemistry in carbon-neutralization technologies. Natl. Sci. Rev. **9** (9), (2025). DOI: https://doi.org/10.1093/nsr/nwac217.

[33] K.K. Pandey, A study of chemical structure of soft and hardwood and wood polymers by FTIR spectroscopy. J. Appl. Polym. Sci. (1999). DOI: https://doi.org/10.1002/(SICI)1097-4628(19990321)71:12<1969::AID-APP6>3.0.CO;2-D

[34] S. Barsberg, Prediction of Vibrational Spectra of Polysaccharides-Simulated IR Spectrum of Cellulose Based on Density Functional Theory (DFT). J. Phys. Chem. B. **114** (36), 11703-11708 (2010). DOI: https://doi.org/10.1021/jp104213z

[35] F. Xu, J. Yu, T. Tesso, F. Dowell, D. Wang, Qualitative and quantitative analysis of lignocellulosic biomass using infrared techniques: A mini-review. Appl. Energ. **104**, 801-809 (2013). DOI: https://doi.org/10.1016/j.apenergy.2012.12.019

[36] S. A. Zaman, S. Ghosh, A generic input–output approach in developing and optimizing an Aspen plus steam-gasification model for biomass. Bioresour. Technol. **337**, 125412 (2021). DOI: https://doi.org/10.1016/j.biortech.2021.125412.

[37] P. Mohanty, K.K. Pant, S.N. Naik, J. Parikh, A. Hornung, J.N. Sahu, Synthesis of green fuels from biogenic waste through thermochemical route – The role of heterogeneous catalyst: A review. Renew. Sustain. Energy Rev. **38**, 131-153 (2014). DOI: https://doi.org/10.1016/j.rser.2014.05.011